Supplemental Information for the Study:

Tertiary lymphoid tissues are microenvironments with intensive interactions between immune cells and proinflammatory parenchymal cells in aged kidneys

Takahisa Yoshikawa[1], Akiko Oguchi[1,2,3], Naoya Toriu[1,3], Yuki Sato[1], Takashi Kobayashi[4], Osamu Ogawa,[4] Hironori Haga[5], Satoko Sakurai[6], Takuya Yamamoto[3,6,7], Yasuhiro Murakawa[2,3,8], Motoko Yanagita[1,3]*

[1]Department of Nephrology, [4]Department of Urology, [5]Department of Diagnostic Pathology, Graduate School of Medicine, Kyoto University, Kyoto, Japan

[2]RIKEN Center for Integrative Medical Sciences, Yokohama, Kanagawa, Japan

[3]Institute for the Advanced Study of Human Biology (WPI-ASHBi), Kyoto University, Kyoto, Japan [6]Department of Life Science Frontiers, Center for iPS Cell Research and Application (CiRA), Kyoto University, Kyoto, Japan

[7]Medical-risk Avoidance based on iPS Cells Team, RIKEN Center for Advanced Intelligence Project (AIP), Kyoto, Japan

[8]IFOM-ETS, Milan, Italy

*To whom correspondence should be addressed:

Motoko Yanagita: Department of Nephrology, Graduate School of Medicine, Kyoto University, Shogoin-Kawahara-cho 54, Sakyo-ku, Kyoto 606-8507, Japan

E-mail: motoy@kuhp.kyoto-u.ac.jp, Tel: +81-75-751-3860, Fax: +81-75-751-3859

Supplemental Material Table of Contents

Supplemental Methods

Supplemental Figures 1–22

Supplemental Figure 15. Immunofluorescence images for transcription factors, p65 and STAT1, in aged injured kidneys with TLTs.

Supplemental Figure 16. *In situ* hybridization images showing high *Stat1* expression within TLTs and their surroundings.

Supplemental Figure 17. Analysis of fibroblasts in the sham-treated kidney.

Supplemental Figure 18. Expression levels of pericyte markers across fibroblast subpopulations in the IRI kidney dataset.

Supplemental Figure 19. KEGG pathways enriched in the fibroblast subpopulations in aged injured kidneys.

Supplemental Figure 20. Expression patterns of selected marker genes from the profibrotic and proinflammatory fibroblasts in aged injured kidneys.

Supplemental Figure 21. Gene expression kinetics during fibroblast differentiation in aged injured kidneys was determined using pseudotime trajectory analysis.

Supplemental Figure 22. Comparison of the expression of proinflammatory fibroblast markers between aged and young injured kidneys.

Supplemental Tables 1–10 (Microsoft Excel format)

Supplemental Table 1. Marker gene lists for each dataset.

Supplemental Table 2. Parameters and the number of nuclei used in the analysis.

Supplemental Table 3. Clinical profiles of two cases after kidney transplantation.

Supplemental Table 4. Enrichment analysis results for PT clusters in aged injured kidneys.

Supplemental Table 5. Regulon activity across the PT clusters in aged injured kidneys. Supplemental Table 6. Differentially expressed genes (DEG) lists of HK-2 cells treated with vehicle, TNFα, and IFNγ.

Supplemental Table 7. Enrichment analysis results for fibroblast clusters in aged injured kidneys.

Supplemental Table 8. Regulon activity across the fibroblast clusters in aged injured kidneys.

Supplemental Table 9. Result of branched expression analysis modeling (BEAM) analysis on the

fibroblast subset in aged injured kidneys.

Supplemental Table 10. Primers for quantitative real-time PCR.

References for Supplemental Information

Supplemental Methods

Renal histochemistry

The mouse kidneys were harvested and cut along the short axis. They were then fixed in 4% paraformaldehyde or 10% neutralized formaldehyde for histological analysis. The kidneys fixed with 10% neutralized formaldehyde were sectioned at 4.0-μm thickness and stained with periodic acid-Schiff (PAS) and Masson's trichrome (MT). The human kidneys were fixed by formalin, embedded by paraffin, sectioned at 4.0-μm thickness.

Immunofluorescence

Immunofluorescence studies of mouse and human kidneys were performed as previously described.[1] Briefly, the kidneys were fixed in 4% paraformaldehyde (PFA) for 6 hours, incubated in 20% sucrose in PBS for 6 hours, and incubated in 30% sucrose in PBS overnight at 4°C. The kidneys were embedded in optimum cutting temperature (OCT) compound (Tissue-Tek O.C.T. Compound, 4853, Sakura Finetek, Tokyo, Japan) and cryosectioned at 6.0-μm thickness and mounted on slides glasses (MAS-01, 83-1881, MATSUNAMI, Osaka, Japan). Formaldehyde-fixed and paraffin-embedded kidney samples were sectioned at a 4.0-μm thickness and used for immunofluorescence analysis. The sections were deparaffinized with xylene and rehydrated with ethanol. Antigen retrieval at 15 minutes at 110°C with the citrate buffer or 10 minutes at 95°C with Dako Target Retrieval Solution, pH 9 (S2367, Dako, Glostrup, Denmark) was performed for deparaffinized and rehydrated sections. These sections were blocked with 5% serum appropriate for secondary antibodies for 1 hour at room temperature and then incubated with primary antibodies for overnight at 4°C. The following antibodies were used for immunofluorescence staining for mouse kidneys: rat anti-B220 (557390, BD PharMingen, San Diego, CA, USA, 1/200), Armenian hamster anti-CD3ε (550275, BD PharMingen, 1/200), goat anti-p75 neurotrophin receptor (p75NTR) (AF1157, R&D Systems, Minneapolis, MN, USA, 1/200), rat anti-KIM1 (14-5861-82, eBioscience, San Diego, CA, USA, 1/200), goat anti-VCAM1 (AF643, R&D Systems, 1/200), goat anti-CXCL9 (AF-492-NA, R&D Systems, 1/200), goat anti-CXCL10 (AF-466-NA, R&D Systems, 1/100), rabbit anti-p105/p50 (13586, Cell Signaling

Technology [CST], Danvers, MA, USA, 1/1000), rabbit anti-STAT1 (9172, CST, 1/500), rabbit anti-phospho-STAT1 (Tyr701) (9167, CST, 1/200), rabbit anti-Tenascin C (ab108930, abcam, Cambridge, UK, 1/200), goat anti-FOXP2 (ab1307, abcam, 1/1000), goat anti-PDGFRβ (AF1042, R&D Systems, 1/200), rat anti-PDGFRβ (14-1402-82, eBioscience, 1/200), goat anti-Type 1 collagen (1310-01, Southern Biotech, Birmingham, AL, USA, 1/200), rabbit anti-Fibronectin (F3648, Sigma-Aldrich, Saint Louis, MO, USA, 1/200), Cy3-conjugated mouse anti α-smooth muscle actin (αSMA) (C6198, Sigma-Aldrich, 1/1000), goat anti-IL33 (AF3626, R&D Systems, 1/8000), rat anti-C3 (1/200), Syrian hamster anti-Podoplanin (14-5381-82, eBioscience, 1/1000), Armenian hamster anti-milk fat globule EGF and factor V/VIII domain containing (MFGE8) (D199-3, Medical & Biological Laboratories [MBL], Tokyo, Japan, 1/200), and rabbit anti-RUNX1 (ab92336, abcam, 1/200). Alexa Fluor 647-conjugated Phalloidin (A22287, Invitrogen, Waltham, MA, USA, 1/500) or Fluorescein-Lotus Tetragonolobus Lectin (LTL) (FL-1321-2, Vector Laboratories, Burlingame, CA, USA, 1/200) was used to stain the PT cells. The following antibodies were used for immunofluorescence staining of human kidneys: rabbit anti-CD3ε (ab5690, abcam, 1/100), mouse anti-CD20 (14-0202-82, eBioscience, 1/200), rabbit anti-Ki67 (ab16667, abcam, 1/200), mouse anti-CD21 (MA5-11417, Invitrogen, 1/100), mouse anti-megalin (sc515772, Santa Cruz, Dallas, TX, USA, 1/200), rabbit anti-VCAM1 (ab134047, abcam, 1/200), goat anti-p75NTR (AF1157, R&D Systems, 1/200), and rabbit anti-phospho-STAT1 (Tyr701) (9167, CST, 1/200). The sections were incubated with secondary antibody including Alexa Fluor 488-, Alexa Fluor 546-, Alexa Fluor 594-, and Cy3-conjugated for 1 hour at room temperature in the dark, counterstained with DAPI, and mounted in mounting medium (Fluoromount, K024, Diagnostic BioSystems, Pleasanton, CA, USA). All of the immunofluorescence samples were analyzed using a confocal microscope (FV1000-D, OLYMPUS, Tokyo, Japan) or an all-in-one fluorescence microscope (BZ-X710, KEYENCE, Osaka, Japan).

Immunohistochemistry

For immunohistochemistry of mouse and human kidneys, formaldehyde-fixed and paraffin-embedded sections were deparaffinized and rehydrated, as described above, for immunofluorescence. After

rehydration, endogenous peroxidase was blocked with 3% H_2O_2, and antigen retrieval was performed as described above for immunofluorescence. The sections were stained with the following primary antibodies: rabbit anti-VCAM1 (39036, CST, 1/200), mouse anti-megalin (sc515772, Santa Cruz, 1/200), rabbit anti-p105/p50 (13586, CST, 1/1000), rabbit anti-p65 (8242, CST, 1/1000), rabbit anti-STAT1 (9172, CST, 1/500), rabbit anti-IRF1 (8478, CST, 1/100), and rabbit anti-phospho-STAT1 (Tyr701) (9167, CST, 1/200). Antibody labeling was detected using a Histofine Simple Stain MAX-PO(R) (414341, NICHIREI BIOSCIENCES, Tokyo, Japan) and a Diaminobenzidine (DAB) Substrate Kit (SK-4100, Vector Laboratories) for rabbit primary antibodies and a Histofine Simple Stain AP(M) (414241, NICHIREI BIOSCIENCES) and an ImmPACT Vector Red Substrate Kit (SK-5105, Vector Laboratories) for mouse primary antibodies. Sections were counterstained using Mayer's Hematoxylin Solution (131-09665, FUJIFILM Wako Pure Chemical Corporation, Osaka, Japan) and mounted in malinol (20091, MUTO PURE CHEMICALS, Tokyo, Japan).

RNAscope *in situ* hybridization

In situ hybridization was performed using an RNAscope Multiplex Fluorescent Assay V2 (323100; Advanced Cell Diagnostics [ACD], Newark, CA, USA) on murine and human kidney samples fixed with 4% paraformaldehyde for 24 hours, embedded in OCT, and cryosectioned at a 10-μm thickness or fixed with 10% neutralized formaldehyde for 24 hours, embedded in paraffin, and sectioned at a 4.0-μm thickness, according to the manufacturer's instructions. The following RNAscope Target Probes were used (all from ACD): Mm-Ccl2 (311791), Mm-Cxcl10 (408921), Mm-Tgfb2 (406181), Mm-Stat1 (479611-C2), Mm-Tnf (481321-C2), Mm-Ifng (311391-C3), Mm-Tnfsf13b (414891), Mm-Pdgfrb (411381-C2), and Hs-CXCL9 (440161).

Reanalysis on single-cell RNA-sequencing dataset for $CD45^+$ immune cells in aged injured kidneys with TLTs

We reused the single-cell RNA-sequencing Seurat object of $CD45^+$ immune cells in aged injured kidneys with TLTs 45 days after a 45-minute ischemia–reperfusion injury (IRI) that we previously

reported.[2] We showed Uniform Manifold Approximation and Projection (UMAP) plots, gene expression patterns of representative marker genes for each cluster using dot plots, and *Cxcr3*, *Tnf*, and *Ifng* expression patterns using violin plots.

Cell culture experiments

HK2 cells, a human PT cell line, were purchased from the American Type Culture Collection (ATCC, Manassas, VA, USA), and C3H10T1/2 cells, mouse embryonic fibroblasts, were purchased from the Health Science Research Resources Bank (HSRRB, Osaka, Japan). HK2 cells were cultured with DMEM/Ham's F-12 (11581-15, Nacalai Tesque, Kyoto, Japan) supplemented with 10% FBS (FBS Standard, CCP-FBS-BR-500, Cosmo Bio, Tokyo, Japan)and penicillin-streptomycin (26253-84, Nacalai Tesque). The cells were treated with recombinant murine TNFα (315-01A, Peprotech, Cranbury, NJ, USA), IFNγ (315-05, Peprotech), or both in DMEM/2.0% FBS for 24 hours at 37°C,and harvested. RNA from the cells was subjected to quantitative real-time PCR analysis. C3H10T1/2 cells were cultured with DMEM (high glucose) (08458-45, Nacalai Tesque) supplemented with 10% FBS and penicillin–streptomycin. They were treated with recombinant murine IFNγ in DMEM/0.5% FBS for 24 hours at 37°C after incubation with DMEM/0.5% FBSfor 12 hours, and then harvested. Their RNA was subjected to quantitative real-time PCR analysis and bulk RNA-sequencing, and their protein was subjected to western blotting (WB) analysis.

Western blotting

Proteins were extracted from C3H10T1/2 cells and WB was performed to screen cells lacking STAT1 protein. Briefly, cells were suspended in RIPA buffer (50 mM Tris-HCl [pH 7.5] [35434-21, Nacalai Tesque], 150 mM NaCl [31320-05, Nacalai Tesque], 1% Nonidet P-40 [145-09701, FUJIFILM Wako Pure Chemical Corporation], and 0.25% sodium dodecyl sulfate [SDS] [191-07145, FUJIFILM Wako Pure Chemical Corporation]), rotated for one hour at 4°C, and centrifuged. After centrifugation, the supernatants were used as total cell lysates. Twenty μg of each sample was applied to SDS-polyacrylamide gel electrophoresis. STAT1 immunoblotting was performed using rabbit anti-STAT1

antibody (9172S, CST, 1/1000). Equal protein loading was confirmed by GAPDH immunoblotting using mouse anti-GAPDH antibody (10R-G109A, Fitzgerald, Acton, MA, USA, 1/4000). The following secondary antibodies were used: horseradish peroxidase (HRP)-linked goat anti-rabbit antibody (7074S, CST, 1/2000) and HRP-linked horse anti-mouse antibody (7076S, CST, 1/5000). The WB bands were captured using a LAS500mini (GE Healthcare, Chicago, IL, USA).

Quantitative real-time PCR

RNA extraction and real-time PCR were performed as described previously.[1] Specific primers were designed using the online tool Primer3Plus (https://www.bioinformatics.nl/cgi-bin/primer3plus/primer3plus.cgi), and the specificity was confirmed using Primer-BLAST (https://www.ncbi.nlm.nih.gov/tools/primer-blast/). The primer sequences are listed in Supplemental Table 10. Expression levels were normalized to those of mouse *Gapdh* or human *GAPDH*.

Supplemental Figure 1

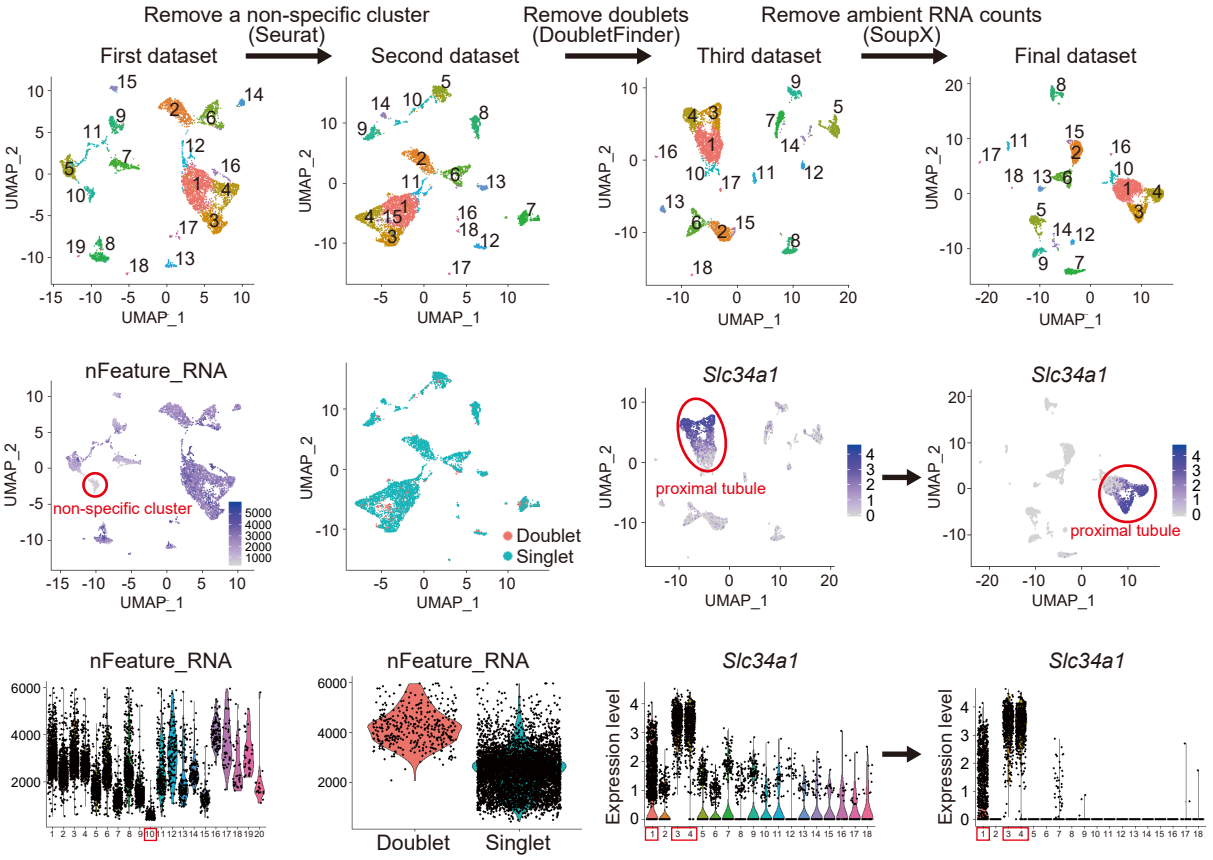

Supplemental Figure 1. Workflow of computational analysis for each dataset. First, the Cell Ranger output "filtered feature matrix" was processed as described in the **Methods** section. The second dataset was generated by removing the non-specific cluster (enclosed with red lines) with the low number of features and without cell type-specific markers from the first dataset using the "subset" function in Seurat. The third dataset was generated by removing estimated doublets from the second dataset using the R package "DoubletFinder". The final dataset was generated by subtracting ambient RNA counts from the third dataset using the R package "SoupX". For example, expression of *Slc34a1*, a PT cell marker, was detected in multiple clusters other than PT clusters (cluster 1, 3, and 4 encircled by led lines) in the third dataset. After subtraction of the ambient RNA counts, *Slc34a1* expression was mostly confined to PT clusters in the final dataset. The detailed process for the computational analysis is described in **Methods** section.

Supplemental Figure 2

A

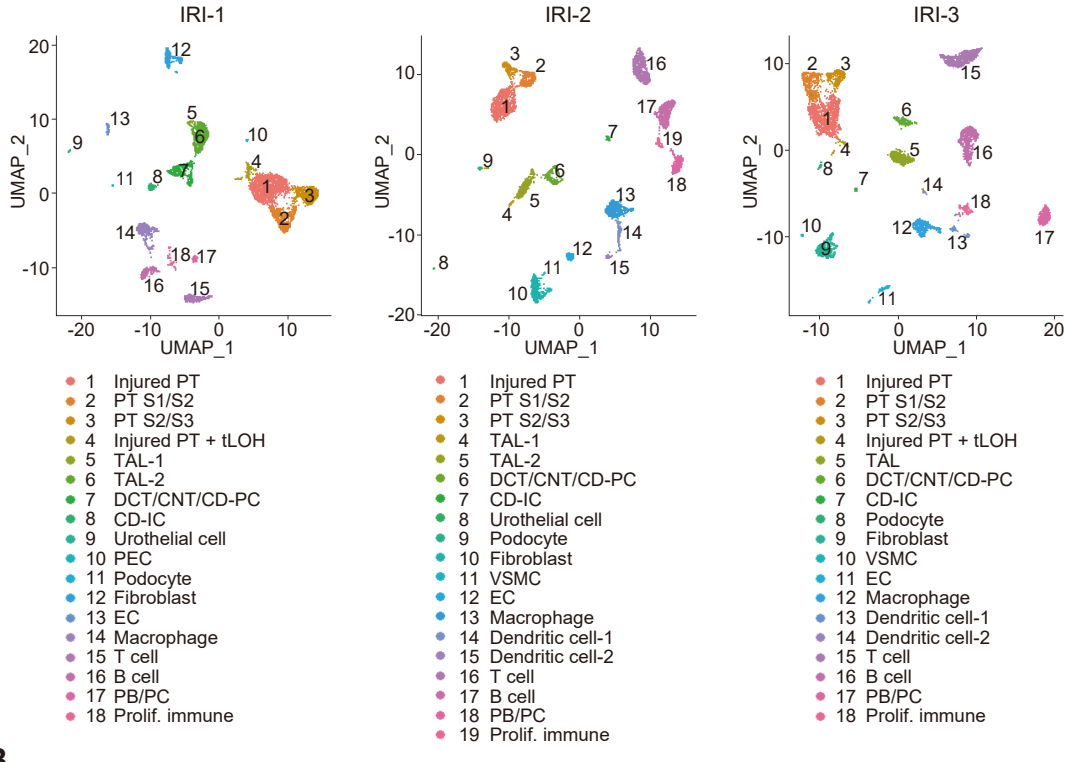

B

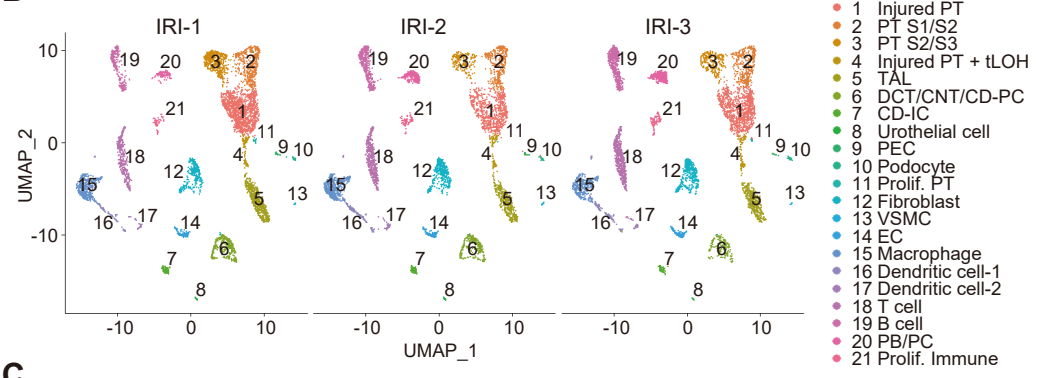

C

Cluster	IRI-1	IRI-2	IRI-3
1	1335	705	994
2	487	353	382
3	488	192	250
4	121	96	116
5	617	365	416
6	415	245	167
7	118	83	60
8	34	22	19
9	33	18	20
10	33	47	56
11	31	2	19
12	315	446	418
13	17	26	26
14	125	143	164
15	415	497	337
16	79	168	168
17	57	69	70
18	380	586	666
19	269	500	597
20	121	338	365
21	60	87	120
total	5550	4988	5430

Supplemental Figure 2. Analysis on each dataset of the three ischemia–reperfusion injury kidneys. (A) Uniform Manifold Approximation and Projection (UMAP) plots for each ischemia–reperfusion injury (IRI) kidney dataset that was analyzed without integration. All datasets included similar cell types. (B) UMAP plots of the integrated IRI kidney dataset separated by the sample of origin (IRI-1, IRI-2, and IRI-3). (C) Tables displaying the number of nuclei included in each cluster in each IRI kidney sample (IRI-1, IRI-2, and IRI-3) in the integrated IRI kidney dataset. Each replicate included all cell types with some differences in the proportions. PT, proximal tubule; S1/S2, S1 segment/S2 segment; S2/S3, S2 segment/S3 segment; tLOH, thin limbs of the loop of Henle; TAL, thick ascending limbs of the loop of Henle; DCT, distal convoluted tubule; CNT, connecting tubule; CD, collecting duct; PC, principal cell; IC, intercalated cell; PEC, parietal epithelial cell; EC, endothelial cell; VSMC, vascular smooth muscle cell; PB/PC, plasmablast/plasma cell; Prolif., proliferating

Supplemental Figure 3

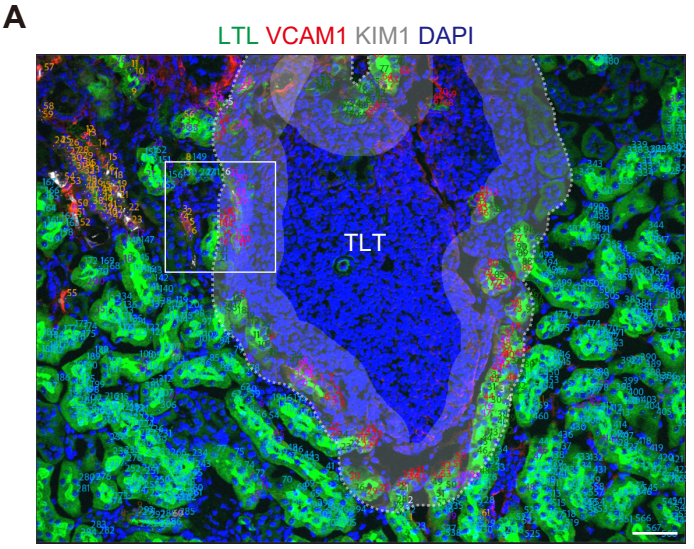

B

	Counts
TLT+KIM1+VCAM1+	33
TLT+KIM1+VCAM1-	6
TLT+KIM1-VCAM1+	88
TLT+KIM1-VCAM1-	99
TLT+ (total)	226

	Counts
TLT-KIM1+VCAM1+	61
TLT-KIM1+VCAM1-	12
TLT-KIM1-VCAM1+	50
TLT-KIM1-VCAM1-	580
TLT- (total)	703

TLT+: PT cells adjacent to TLTs
TLT-: PT cells not adjacent to TLTs

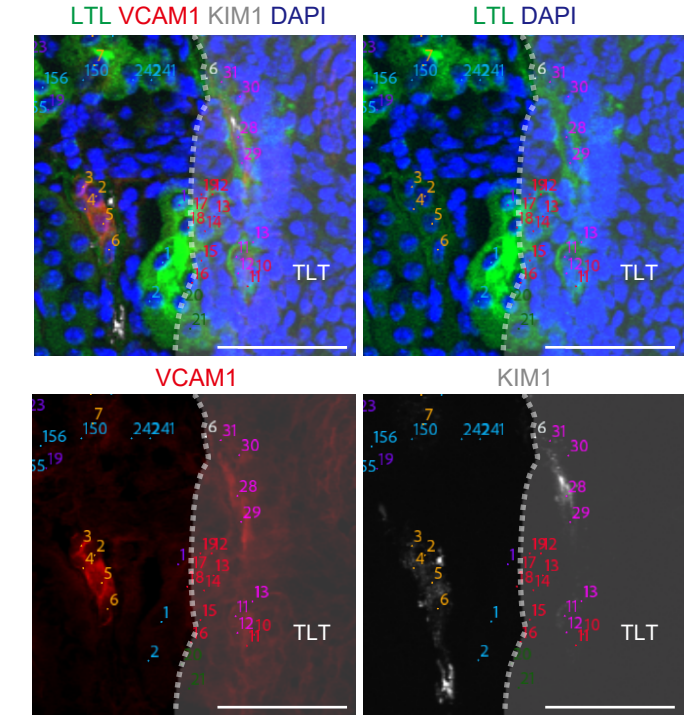

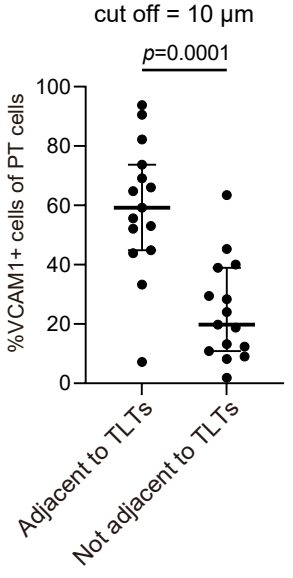

Supplemental Figure 3. Representative images used to count VCAM1⁺ or KIM1⁺ PT cells in injured kidneys. (A–C) Immunofluorescence images of PTs stained using LTL (green), VCAM1 (red), KIM1 (gray), and DAPI (blue). (A) All PT cells were classified into eight types based on whether they were adjacent to TLTs (within 35 μm from the TLT boundaries, the area within the outer dashed line of the translucent band) and the staining pattern for VCAM1 and KIM1. They were counted using colored numbers based on their classification. (B) Tables showing the number of PT cells in each classification in the representative image in (A). (C) Magnified images of the area enclosed with a square in (A). Scale = 50 μm. (D) Quantification of the percentages of VCAM1⁺ PT cells among "PT cells adjacent to TLTs" or "PT cells not adjacent to TLTs" with setting the cutoff distance from TLT borders to 10 μm, in each region of interest (ROI) in mild IRI model, using three ROIs including TLTs per kidney section (n = 5, total of 15 ROIs). With this cutoff, VCAM1⁺ PT cells were also significantly more prevalent around TLTs than in the other area (p = 0.0001). Data are shown as the median and interquartile range. Mann–Whitney test was used to analyze the difference.

Supplemental Figure 4

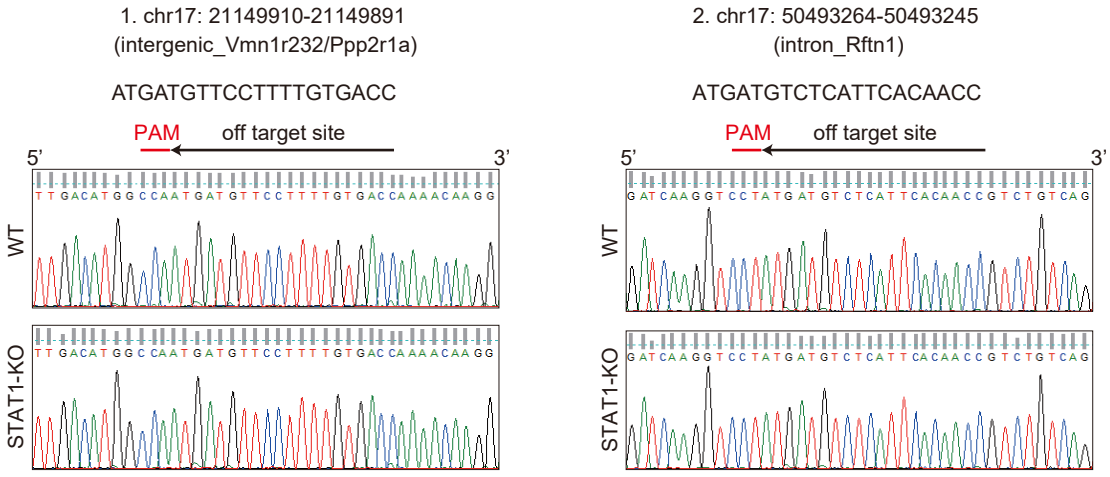

Supplemental Figure 4. Sanger sequence analysis of off-targets of wild-type and STAT1-knockout C3H10T1/2 cells. Sanger sequence analysis on the two representative potential off target sites with the highest Cutting Frequency Determination (CFD) scores calculated by CRISPOR demonstrated no mutation in STAT1-knockout (KO) C3H10T1/2 cells (1; intergenic_Vmn1r232/Ppp2r1a, 2; intron_Rftn1).[3] (red line, protospacer adjacent motif (PAM) sequence; black arrow, off target site sequence)

Supplemental Figure 5

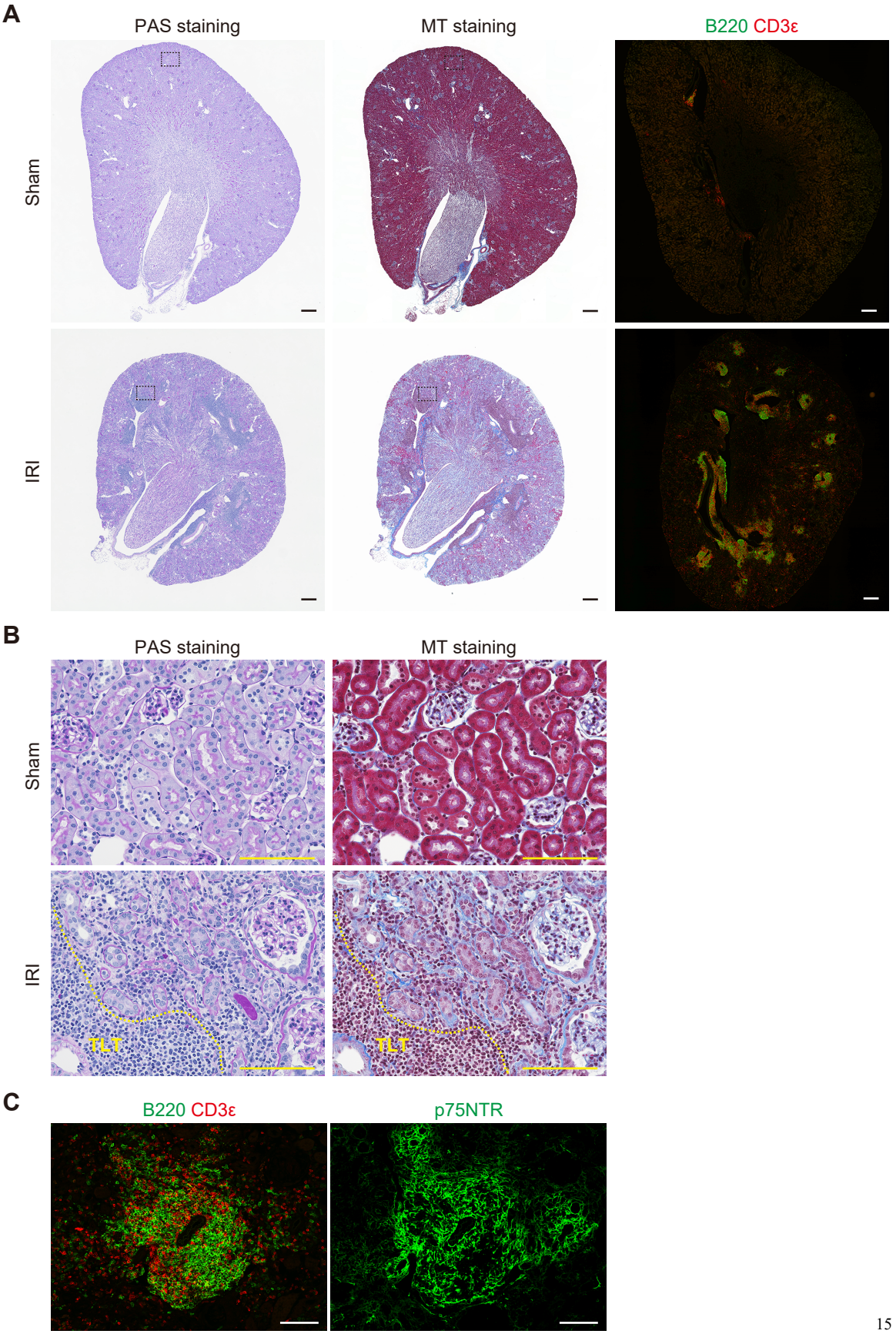

Supplemental Figure 5. Histology of mouse kidneys 30 days after sham surgery and 45-minute ischemia–reperfusion injury (IRI). (A) Periodic acid–Schiff (PAS) staining, Masson–Trichrome (MT) staining, and immunofluorescence staining for B220 (green) and CD3ε (red) of a murine kidney 30 days after sham surgery and IRI, which was used for snRNA-seq. The kidney after IRI showed multiple TLTs and extensive fibrosis. Scale bars = 300 μm. (B) The areas enclosed by dashed lines in (A) were magnified. Tubular atrophy and interstitial fibrosis were identified in aged injured kidneys after IRI. TLT borders were shown as yellow dashed lines. Scale bars = 100 μm. (C) Representative immunofluorescence images of TLTs staining for B220 (green) and CD3ε (red), markers for B cells and T cells, respectively, and for p75 neurotrophin receptor (p75NTR) (green), a marker for fibroblasts within TLTs. Scale bars = 100 μm.

Supplemental Figure 6

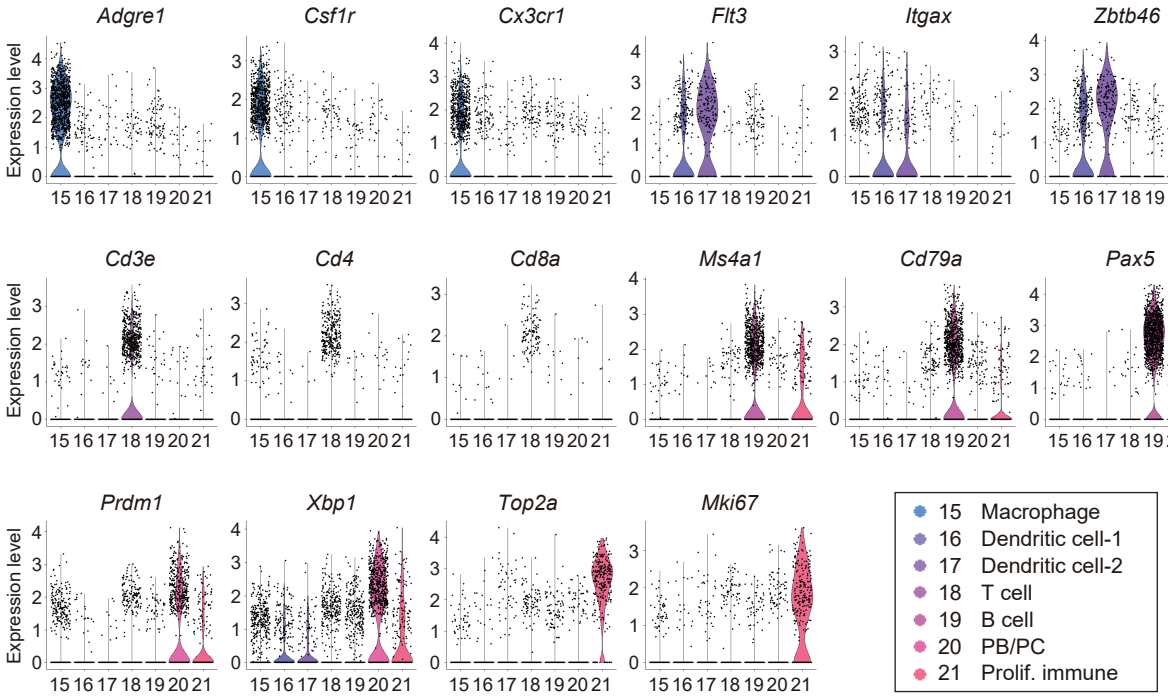

Supplemental Figure 6. Expression patterns of well-known marker genes across immune cells in the ischemia–reperfusion injury (IRI) kidneys. Violin plots showing expression patterns of the well-known marker genes for each immune cell type across immune cell clusters in the IRI kidney dataset (cluster 15–21 in Figure 1D). *Adgre1*, *Csf1r*, and *Cx3Cr1* are used as macrophage markers, *Flt3*, *Itgax*, and *Zbtb46* as dendritic cell markers, *Cd3e*, *Cd4*, and *Cd8a* as T cell markers, *Ms4a1*, *Cd79a*, and *Pax5* as B cell markers, *Prdm1* and *Xbp1* as plasmablast/plasma cell (PB/PC) markers, and *Top2a* and *Mki67* as proliferating (Prolif.) cell markers.

Supplemental Figure 7

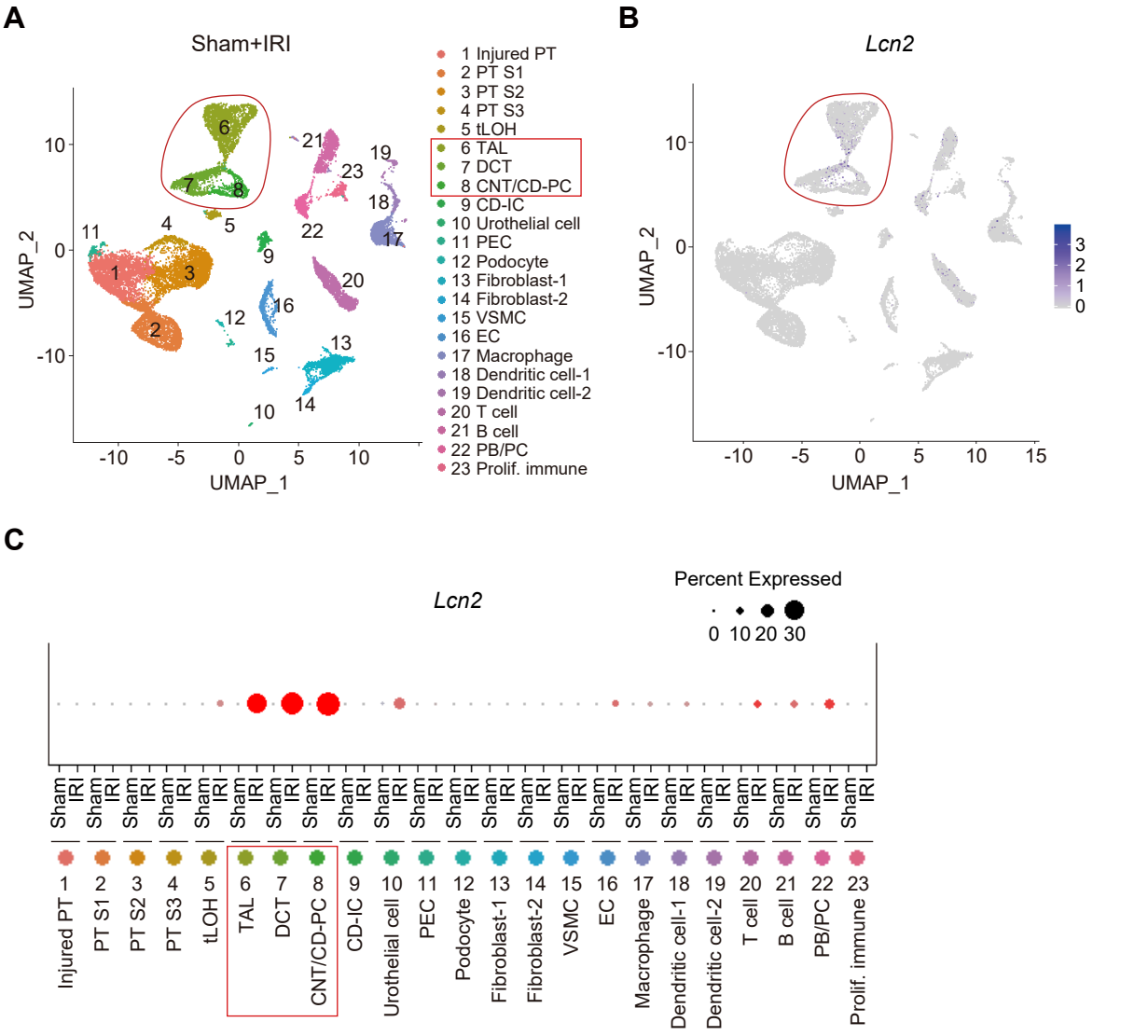

Supplemental Figure 7. Injured distal nephrons with upregulated *Lcn2* expression in the ischemia–reperfusion injury (IRI) kidneys. (A) Uniform Manifold Approximation and Projection (UMAP) plots of the integrated dataset of the sham-treated and three IRI kidneys (the same as UMAP plots in Figure 1E). Distal nephron clusters (cluster 6–8) were encircled by red lines. (B) Feature plots showing gene expression of *Lcn2* encoding Ngal in the integrated dataset of a sham-treated and three IRI kidneys. Clusters 6–8 were encircled by red lines. (C) Dot plots showing the percentage of cells expressing *Lcn2* in each cluster separated by the sample types. PT, proximal tubule; S1, S1 segment; S2, S2 segment; S3, S3 segment; tLOH, thin limbs of the loop of Henle; TAL, thick ascending limbs of the loop of Henle; DCT, distal convoluted tubule; CNT, connecting tubule; CD, collecting duct; PC, principal cell; IC, intercalated cell; PEC, parietal epithelial cell; VSMC, vascular smooth muscle cell; EC, endothelial cell; PB/PC, plasmablast/plasma cell; Prolif., Proliferating

Supplemental Figure 8

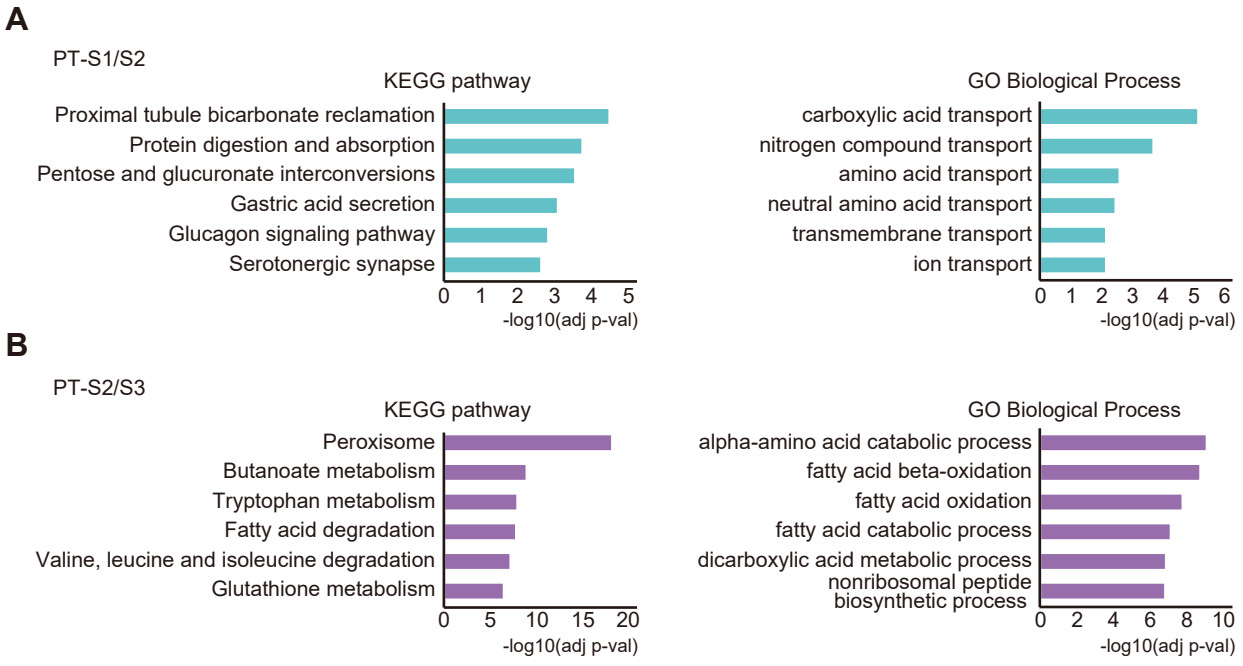

Supplemental Figure 8. Enrichment analysis of the reclustered PT clusters in the ischemia–reperfusion injury kidney dataset. (A, B) Enrichment analysis on the marker genes of (A) PT-S1/S2 and (B) PT-S2/S3 clusters in the PT subset in the integrated ischemia–reperfusion injury (IRI) kidney dataset was performed. Top six KEGG pathways and GO terms are shown in the bar graphs. Significance was expressed as $-\log_{10}$(adjusted *p*-value). PT, proximal tubule; S1/S2, S1 segment/S2 segment; S2/S3, S2 segment/S3 segment

Supplemental Figure 9

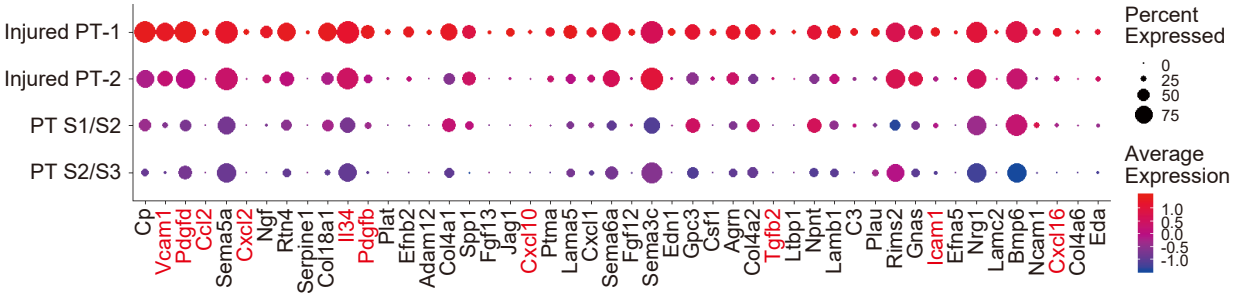

Supplemental Figure 9. Expression patterns of the genes encoding ligands highly expressed in the injured PT-1. Dot plots showing expression patterns of the genes encoding ligands highly expressed in injured PT-1 across the four PT clusters in the ischemia–reperfusion injury kidney dataset. Expression patterns of the genes that are shown in red characters are also shown in the violin plots in Figure 2C.

Supplemental Figure 10

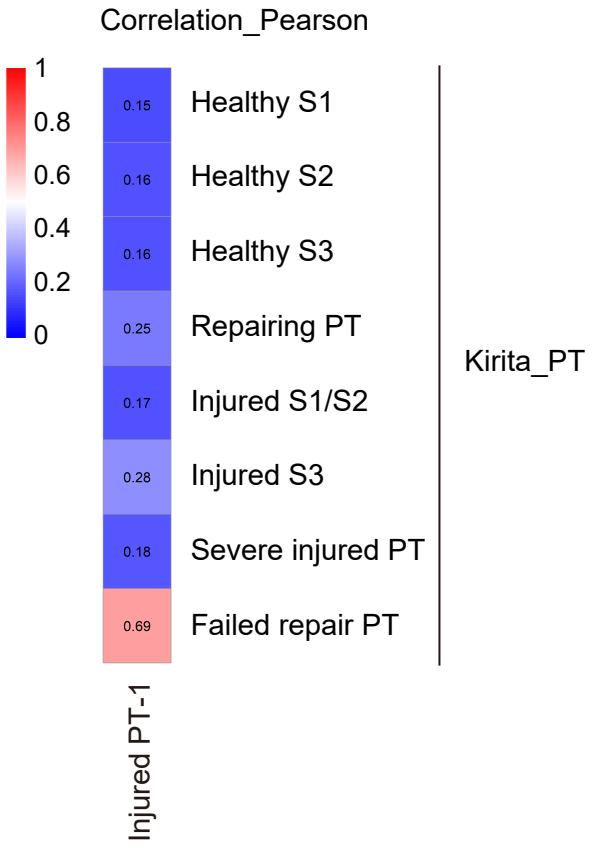

Supplemental Figure 10. Pearson correlation analysis between the injured PT-1 in our analysis and PT subpopulations in previous publiation. The heatmap showed Pearson correlation coefficient calculated between injured PT-1 and seven PT subpopulations in previous publication by Kirita et al.[4] (Kirita_PT), based on the average expression profiles of marker genes for PT subpopulations in our data. Injured PT-1 in our data was shown to be the most similar to “Failed repair PT” in Kirita_PT. PT, proximal tubule; S1, S1 segment; S2, S2 segment; S3, S3 segment

Supplemental Figure 11

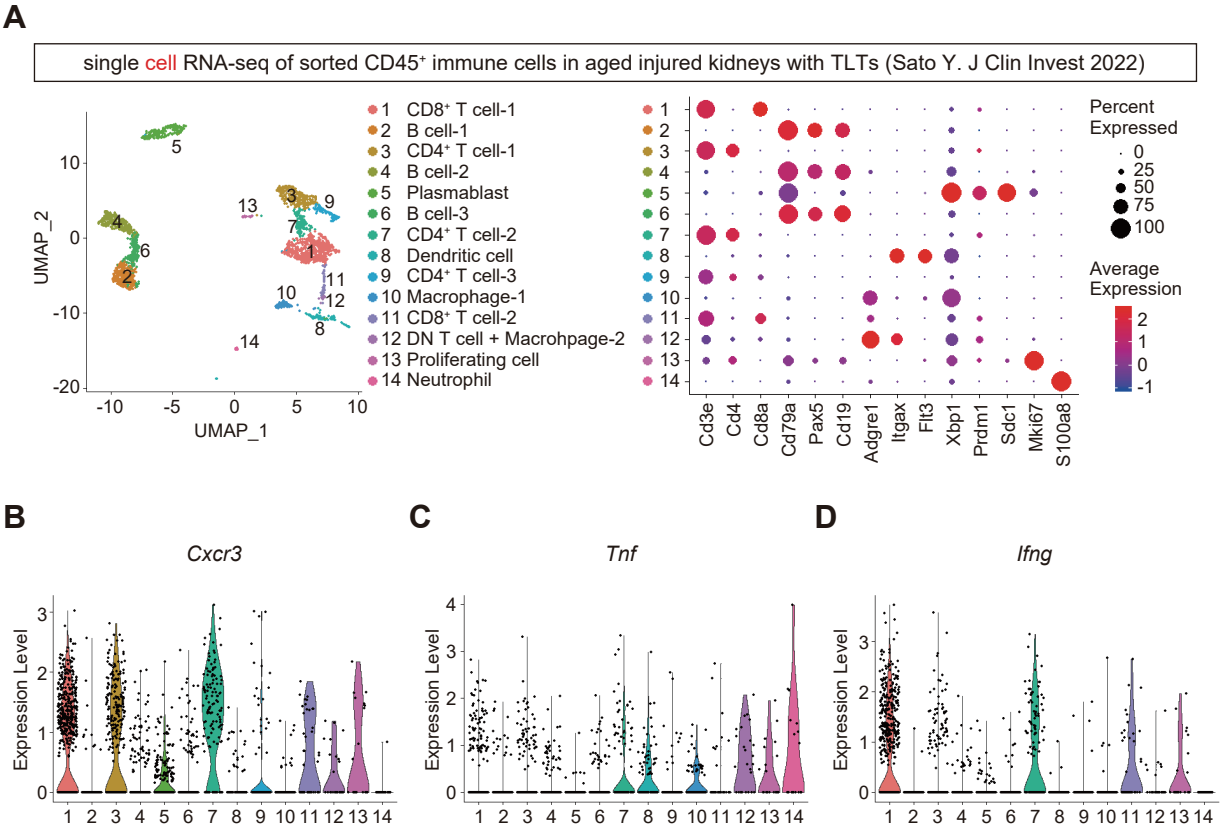

Supplemental Figure 11. Expression patterns of *Cxcr3*, *Tnf*, and *Ifng* in immune cells in aged injured kidneys with TLTs based on scRNA-seq dataset. (A) Uniform Manifold Approximation and Projection (UMAP) plots displaying the clustering of the sorted CD45+ immune cells in aged injured kidneys with TLTs and dot plots displaying expression patterns of the representative marker genes for each cluster based on scRNA-seq dataset that we previously reported.[2] (B–D) Violin plots showing gene expression patterns of (B) *Cxcr3*, (C) *Tnf*, and (D) *Ifng* in immune cells in the aged injured kidneys with TLTs detected by scRNA-seq dataset.[2] DN double negative

Supplemental Figure 12

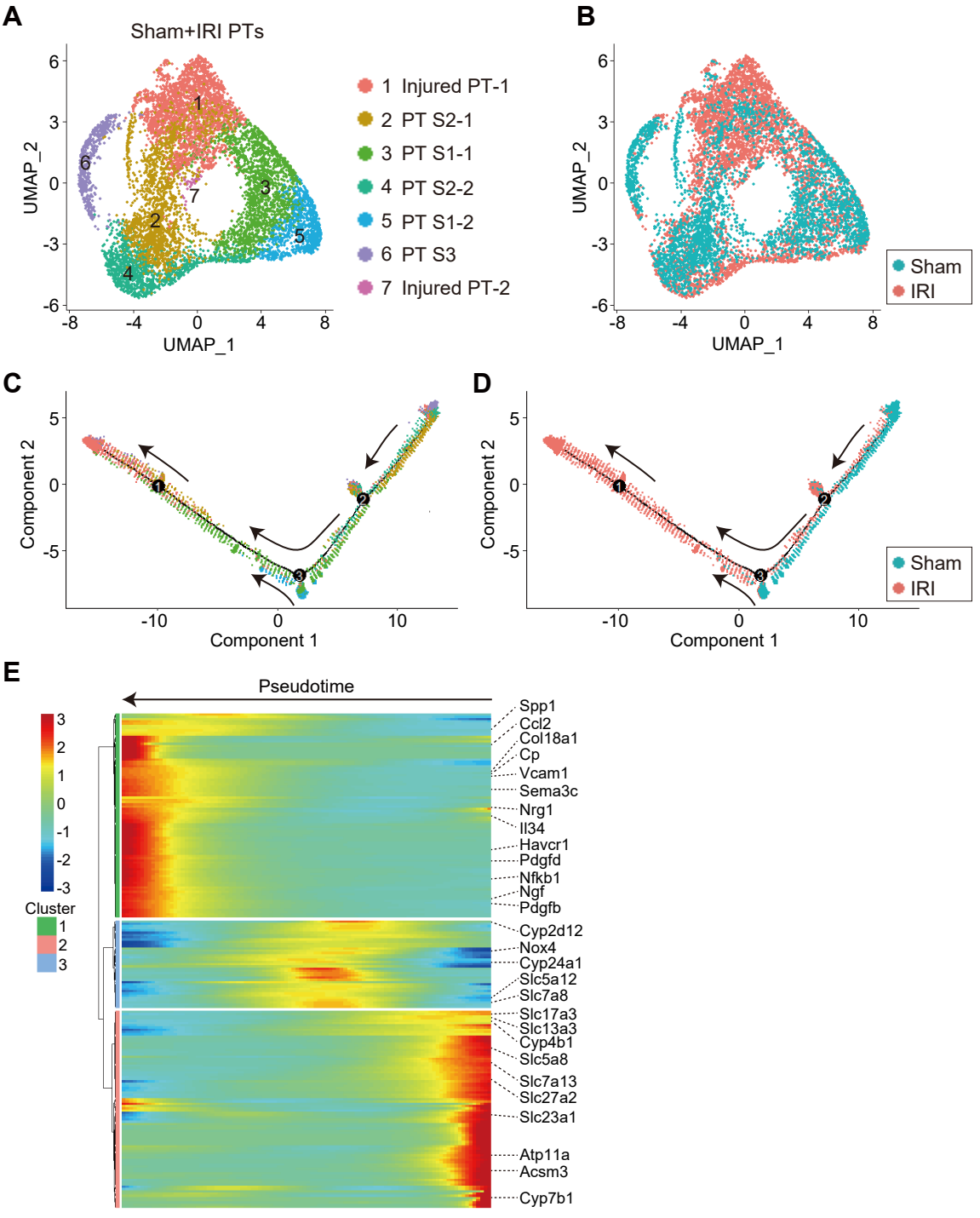

Supplemental Figure 12. Trajectory analysis of PT subsets. (A) Uniform Manifold Approximation and Projection (UMAP) plots showed that the integrated data of PT subsets in sham-treated and ischemia–reperfusion injury (IRI) kidney datasets was classified into seven clusters. (B) The UMAP plots were colored by sample types, sham (blue dots) and IRI (red dots). (C) Pseudotime trajectory analysis was performed on the integrated PT dataset using Monocle2. (D)The trajectory plots were colored by sample types, sham (blue dots) and IRI (red dots). (E) A heatmap showing gene expression changes of the representative marker genes for PT subpopulations, demonstrating that injured PT marker genes were upregulated with the downregulation of healthy PT marker genes along pseudotime.

Supplemental Figure 13

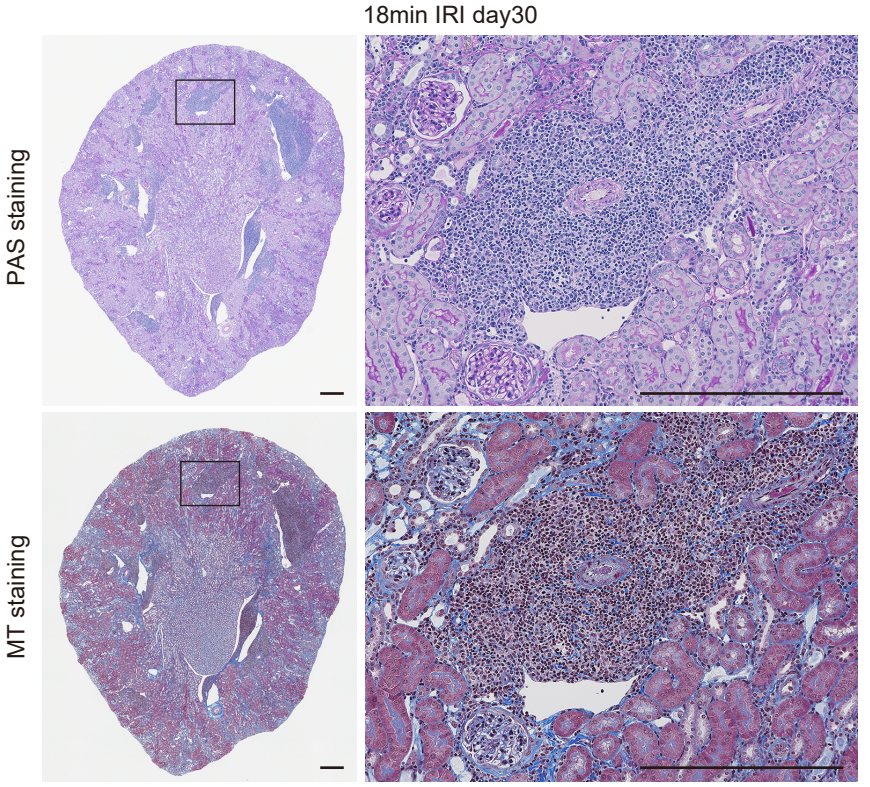

Supplemental Figure 13. Histology of aged injured kidneys 30 days after 18-minute mild ischemia–reperfusion injury. Periodic acid–Schiff (PAS) staining and Masson–Trichrome (MT) staining of murine kidneys 30 days after 18-minute mild ischemia–reperfusion injury (IRI). The right panels show the magnified images for the regions enclosed by rectangles in the left panels. Scale bars = 300 μm.

Supplemental Figure 14

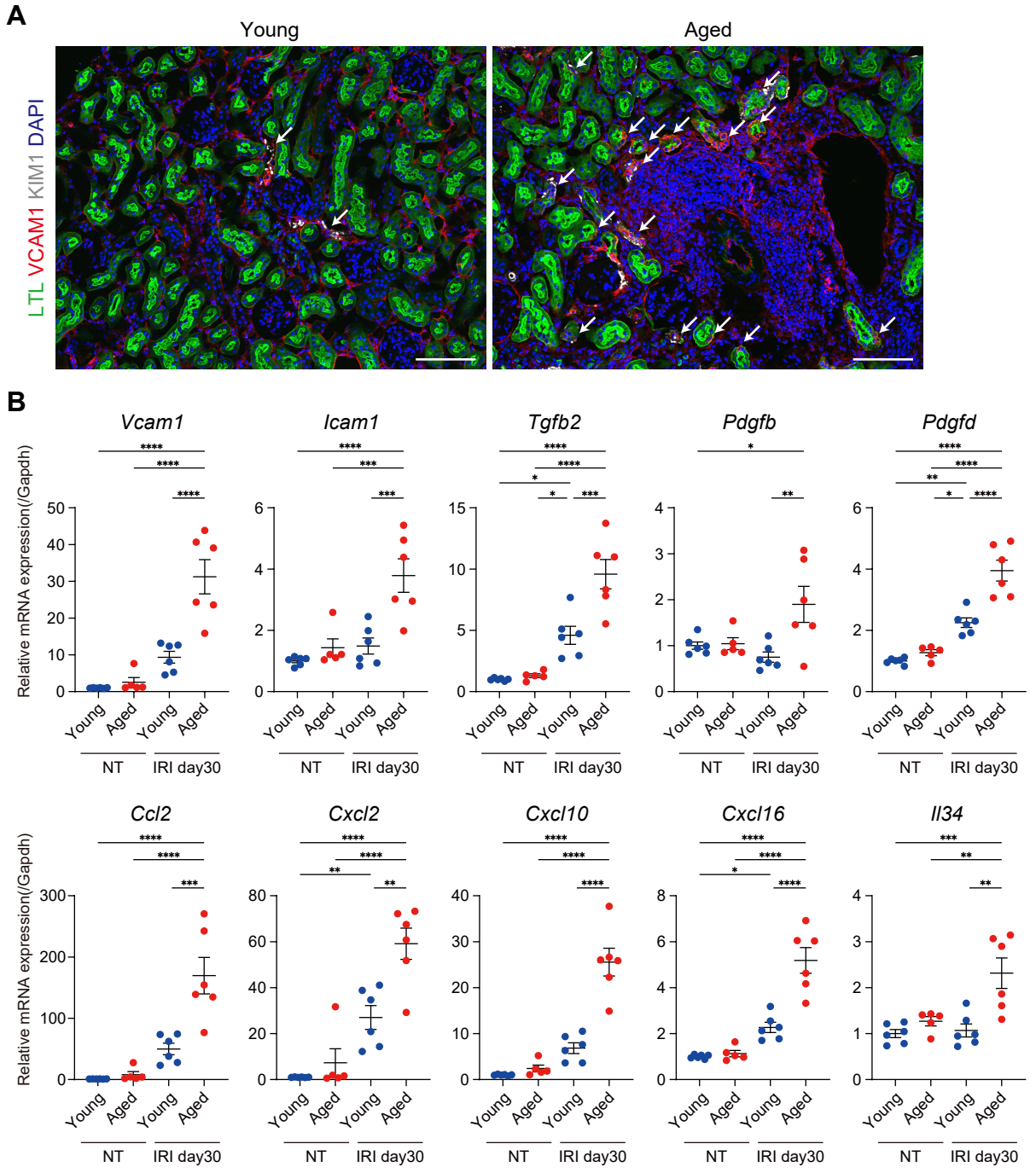

Supplemental Figure 14. Comparison of the expression of injured PT markers between aged and young injured kidneys. (A) Representative immunofluorescence images of LTL (green), VCAM1 (red), KIM1 (gray), and DAPI (blue) in young and aged injured kidneys 30 days after 18-min ischemia–reperfusion injury (IRI). VCAM1$^+$ injured PTs (arrows) were more abundant in aged kidneys than young kidneys. Interstitial cells also expressed VCAM1. Scale bars = 100 μm. (B) Results of quantitative real-time PCR for young and aged non-treated (NT) kidneys and injured kidneys 30 days after 18-min IRI (n = 5–6/group). Relative mRNA expressions of injured PT markers were shown. The expression levels were normalized to those of *Gapdh*. Values were shown as mean ± standard error (SE). Statistical significance was determined using a one-way analysis of variance (ANOVA) followed by the Tukey–Kramer post-hoc test (*p < 0.05, **p < 0.01, ***p < 0.001, and ****p < 0.0001).

Supplemental Figure 15

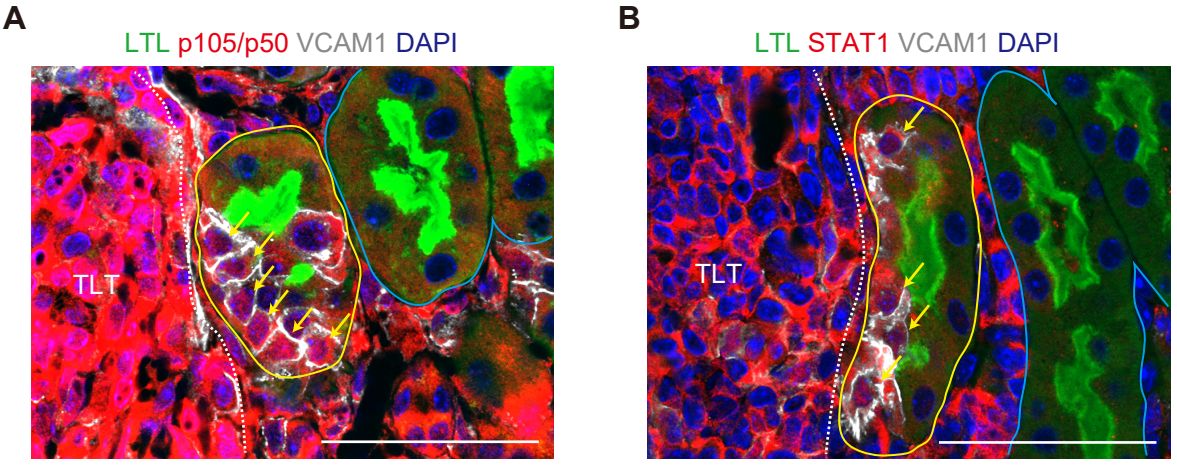

Supplemental Figure 15. Immunofluorescence images for transcription factors, p65 and STAT1, in aged injured kidneys with TLTs. (A, B) Immunofluorescence images of LTL (green), (A) p105/p50 (red), (B) STAT1 (red), VCAM1 (gray), and DAPI (blue) in the mild IRI kidneys. The VCAM1^{+} injured PT cells with upregulated expressions of p105/p50 and STAT1 adjacent to TLTs are shown by yellow arrows. The VCAM1^{+} PTs and VCAM1^{-} PTs are enclosed by yellow and light blue solid lines, respectively. TLT borders are shown as white dashed lines. Scale bars = 50 μm.

Supplemental Figure 16

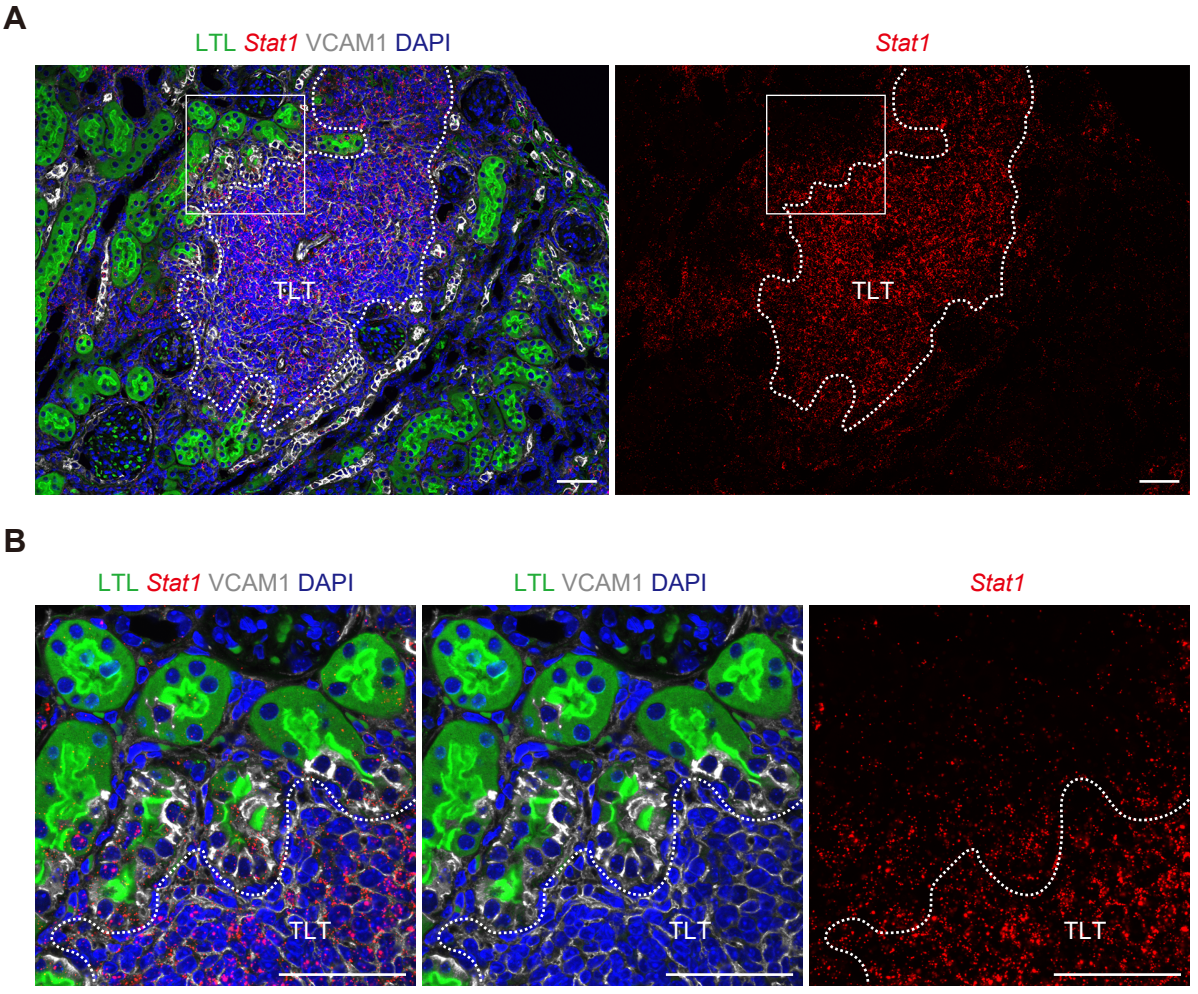

Supplemental Figure 16. *In situ* hybridization images showing high *Stat1* expression within TLTs and their surroundings. (A, B) A combination of *in situ* hybridization (*Stat1* [red]) and immunofluorescence (LTL [green], VCAM1 [gray], and DAPI [blue]) displayed high *Stat1* expression within TLTs as well as in VCAM1^{+} injured PT cells adjacent to TLTs (A) in low magnification. The area enclosed by squares in (A) are magnified in (B). Scale bars = 50 μm.

Supplemental Figure 17

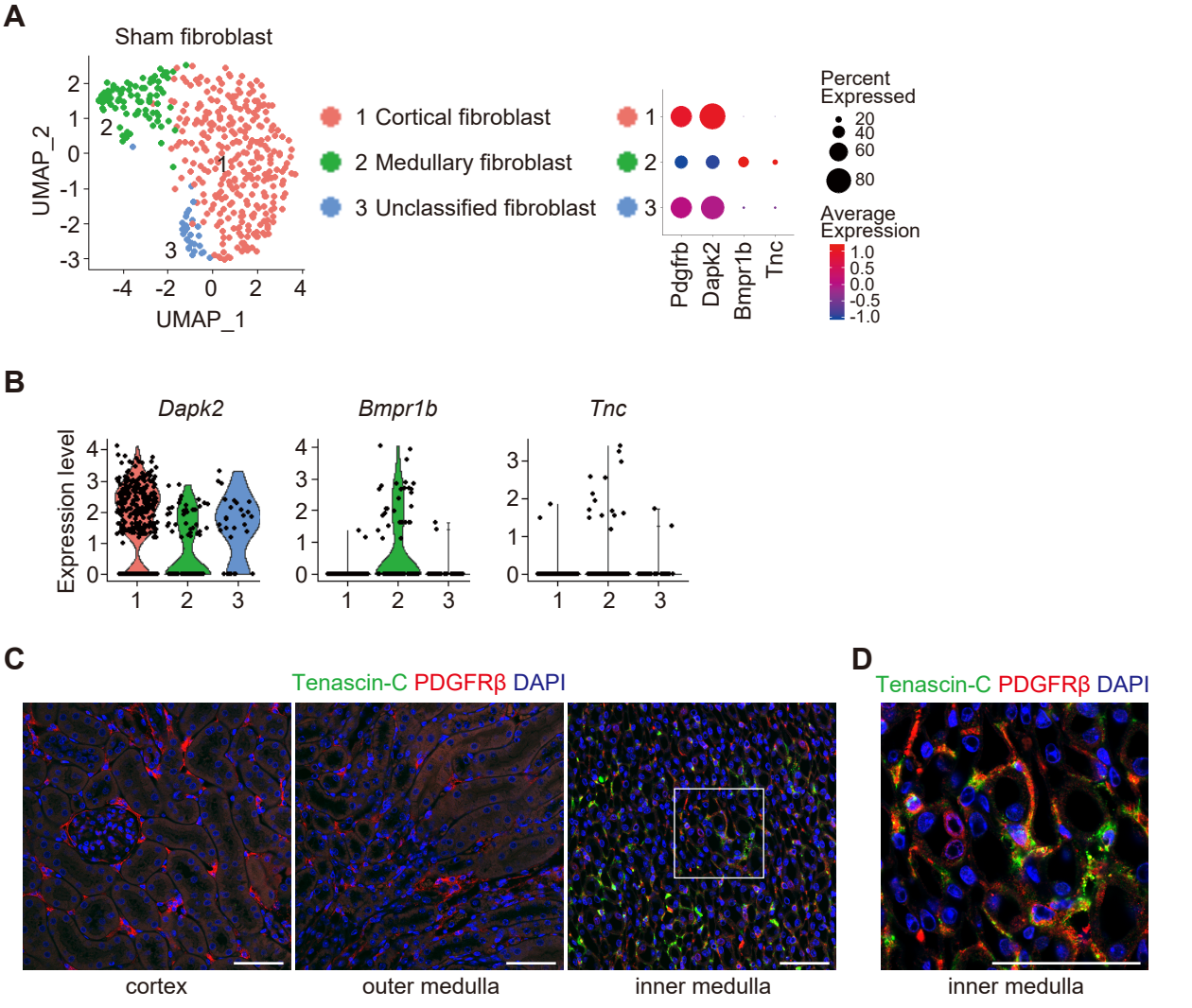

Supplemental Figure 17. Analysis of fibroblasts in the sham-treated kidney. (A) Uniform Manifold Approximation and Projection (UMAP) plots displaying reclustered fibroblast clusters in the sham-treated kidney and dot plots showing expression patterns of the selected marker genes for each cluster. (B) Violin plots showing the expression of the selected marker genes (*Dapk2*, *Bmpr1b*, and *Tnc*) across three fibroblast clusters. (C, D) Immunofluorescence staining of Tenascin-C (green), PDGFRβ (red), and DAPI (blue) in the cortex, outer medulla, and inner medulla of the sham-treated kidney. Tenascin-C was stained in the PDGFRβ^{+} fibroblasts in the inner medulla in the sham-treated kidney (C). The area enclosed by a square in (C) is magnified in (D). Scale bars = 50 μm.

Supplemental Figure 18

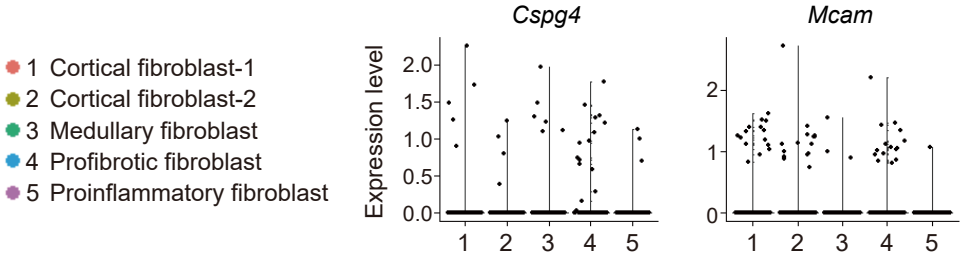

Supplemental Figure 18. Expression levels of pericyte markers across fibroblast subpopulations in the ischemia–reperfusion injury kidney dataset. The violin plots showed that gene expression of pericyte markers such as *Cspg4* and *Mcam* (encoding NG2 and CD146, respectively) was scarce across all clusters.

Supplemental Figure 19

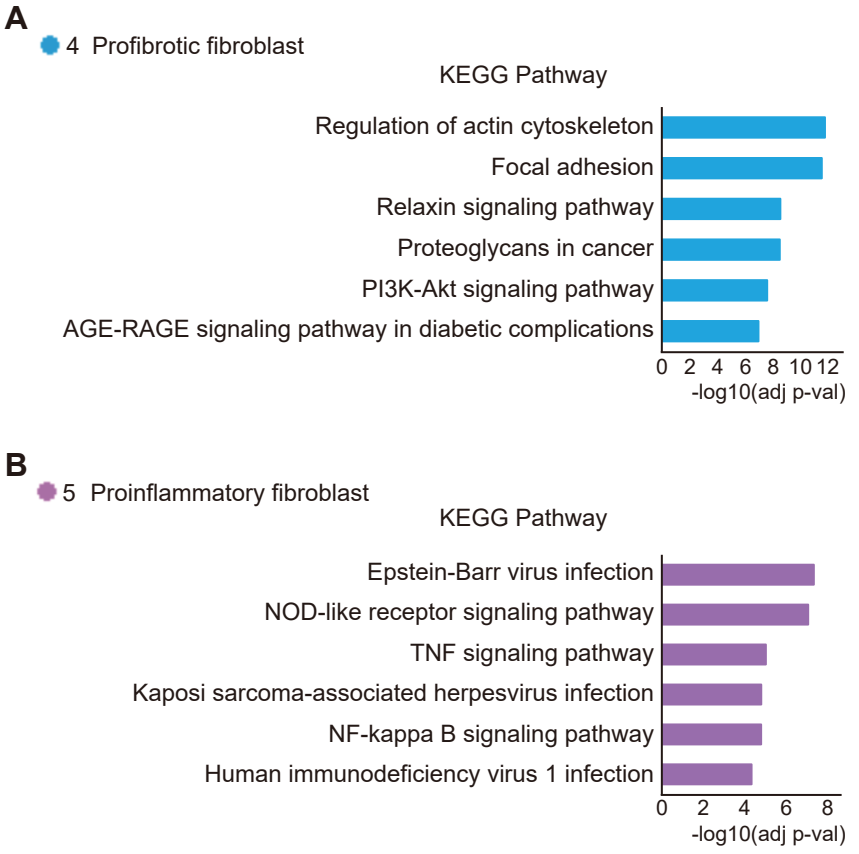

Supplemental Figure 19. KEGG pathways enriched in the fibroblast subpopulations in aged injured kidneys. (A, B) Top six KEGG pathways significantly enriched in the profibrotic (cluster 4 in Figure 5A) and proinflammatory (cluster 5 in Figure 5A) fibroblast cluster in aged injured kidneys. Significance was shown as $-\log_{10}$(adjusted *p*-value).

Supplemental Figure 20

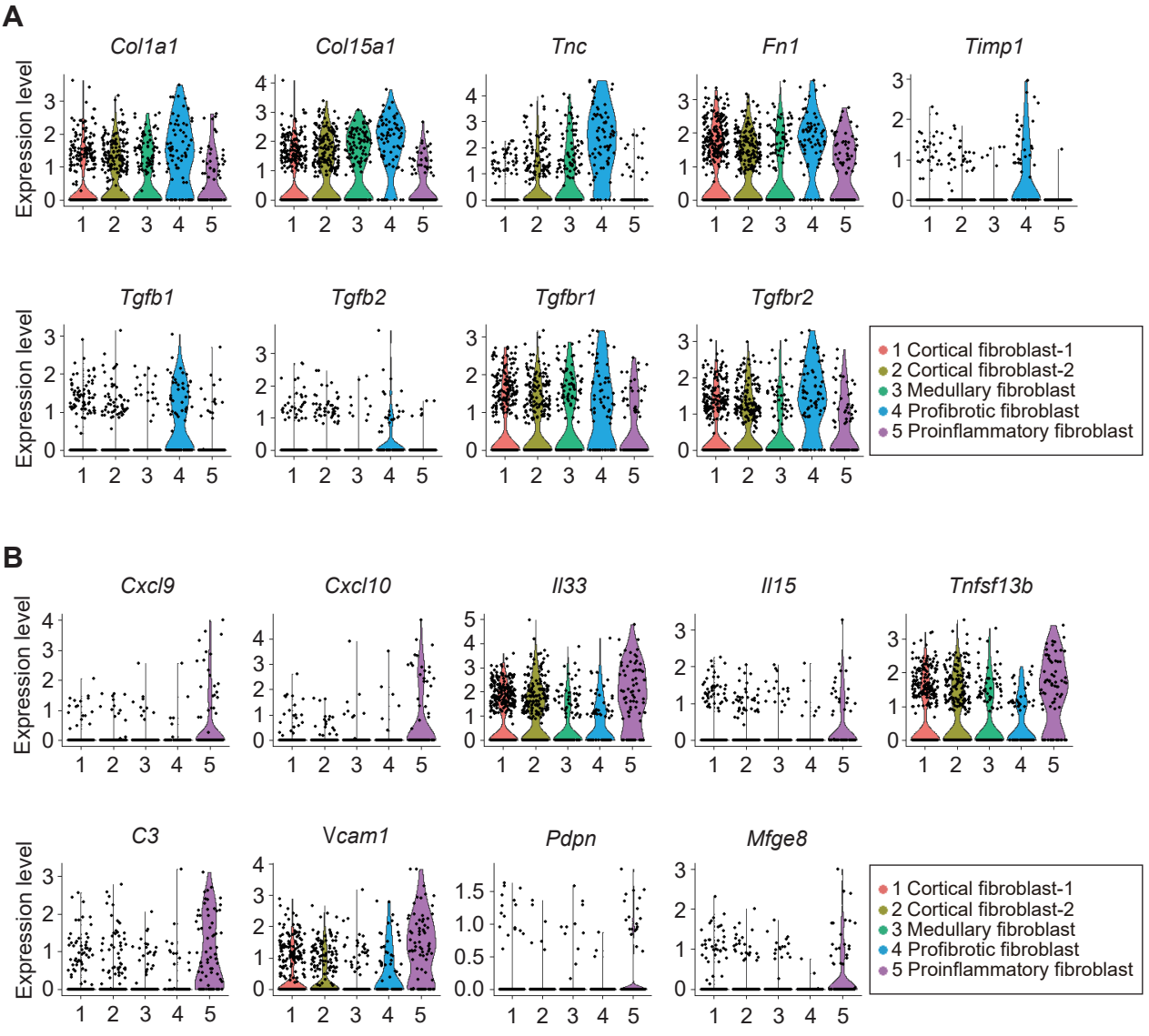

Supplemental Figure 20. Expression patterns of selected marker genes from the profibrotic and proinflammatory fibroblasts in aged injured kidneys. (A, B) Violin plots displaying expression patterns of the selected marker genes from the (A) profibrotic and (B) proinflammatory fibroblasts across the five fibroblast clusters in aged injured kidneys.

Supplemental Figure 21

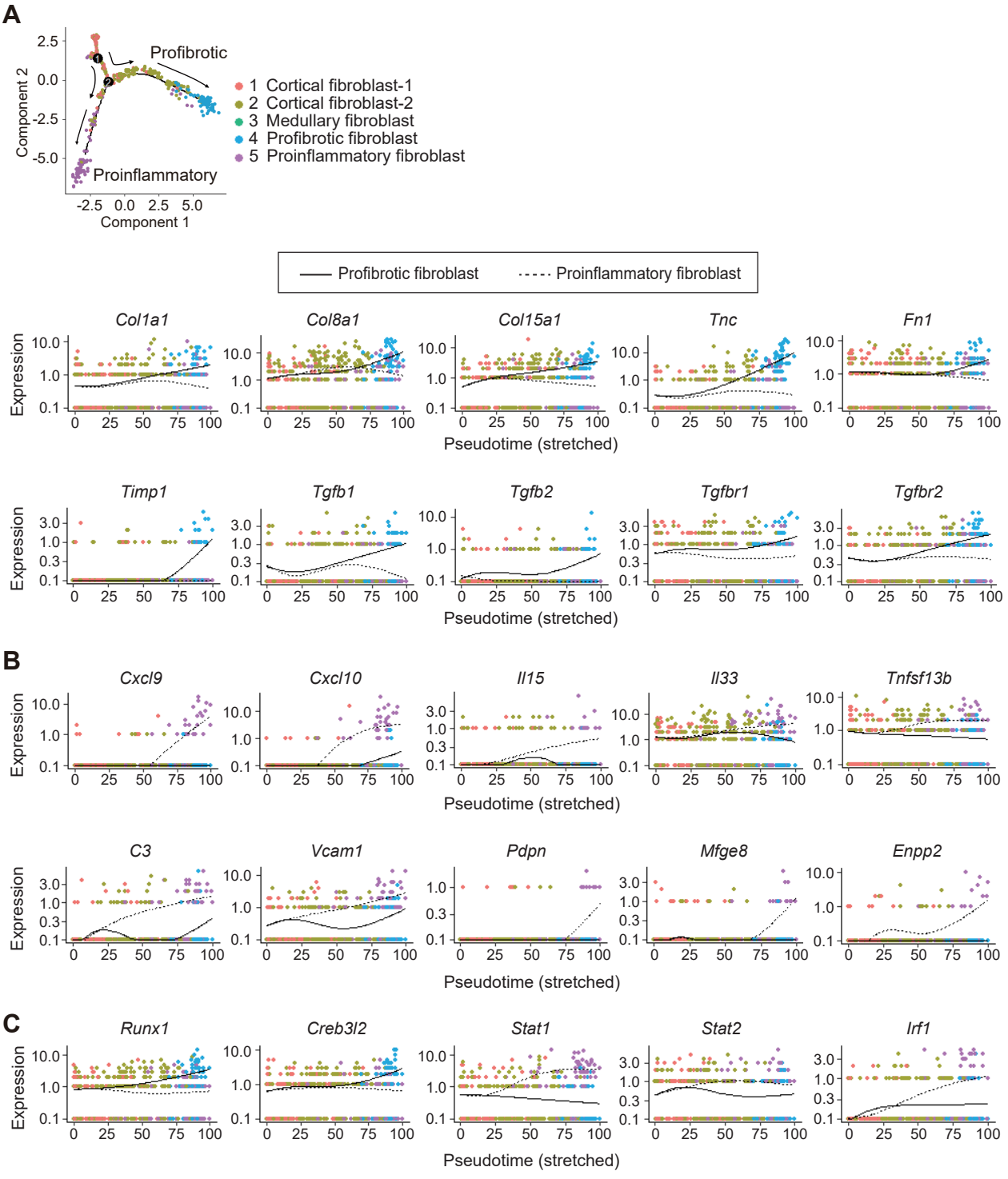

Supplemental Figure 21. Gene expression kinetics during fibroblast differentiation in aged injured kidneys was determined using pseudotime trajectory analysis. (A–C) The plots showing the gene expression level kinetics during renal fibroblast differentiation into profibrotic subtypes (solid lines) and into proinflammatory subtypes (dashed lines) along pseudotime from node number 2 in the trajectory plots in (A). The trajectory plots in (A) is the same as the plots in Figure 5G. The gene expression kinetics of (A) marker genes for the profibrotic fibroblasts, (B) marker genes for the proinflammatory fibroblasts, and (C) transcription factors activated in each fibroblast cluster are displayed.

Supplemental Figure 22

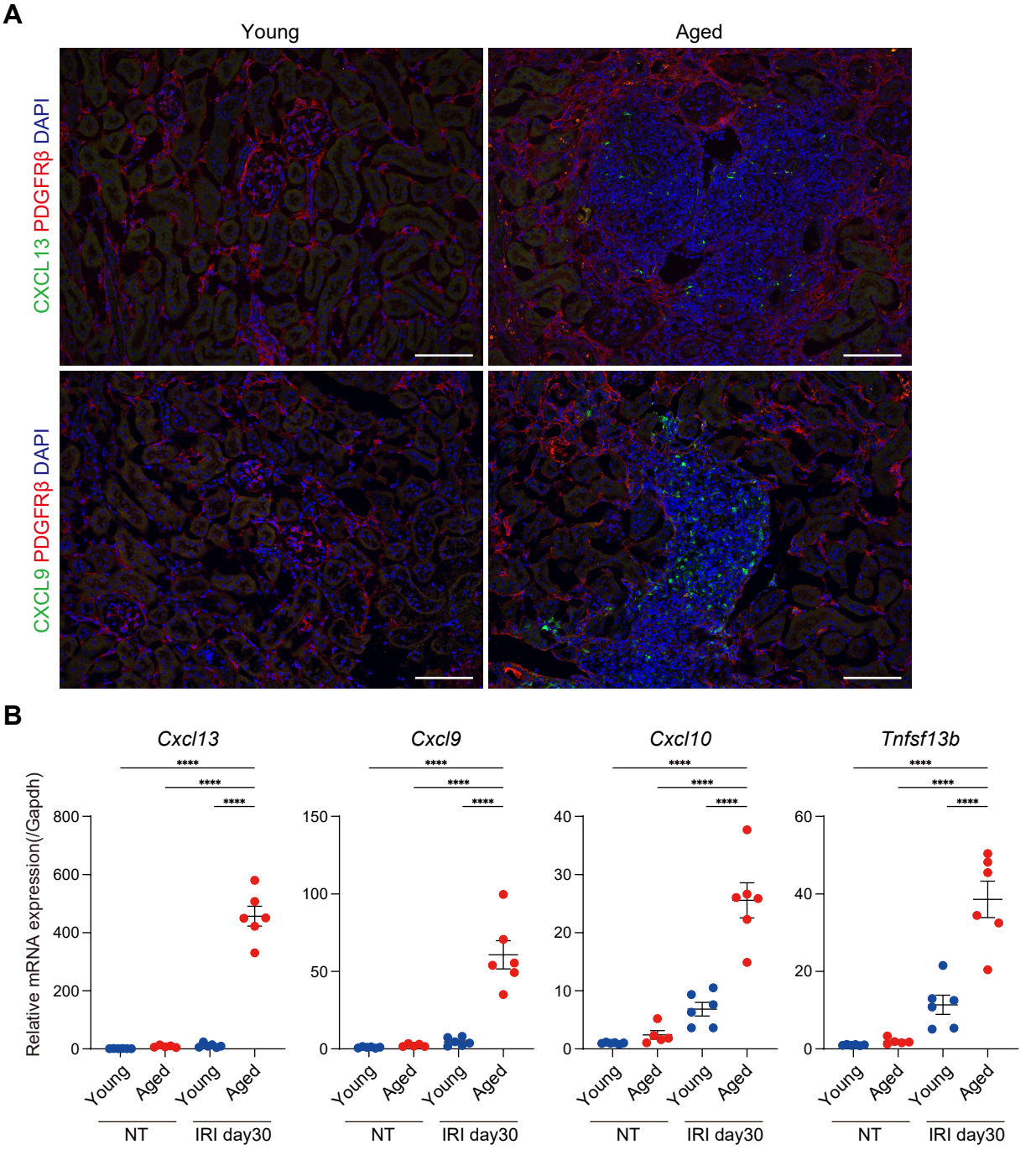

Supplemental Figure 22. Comparison of the expression of proinflammatory fibroblast markers between aged and young injured kidneys. (A) Representative immunofluorescence images staining for CXCL13 (green), CXCL9 (green), PDGFRβ (red), and DAPI (blue) showed more abundant expression of these chemokines in the aged injured kidneys with TLTs 30 days after 18-min ischemia–reperfusion injury (IRI). Scale bars = 100 μm. (B) Results of quantitative real-time PCR for young and aged non-treated (NT) and injured kidneys (n = 5–6/group). Relative mRNA expressions of chemokines and cytokines expressed by the proinflammatory fibrobalsts were shown. The expression levels were normalized to those of *Gapdh*. Values were shown as mean ± standard error (SE). Statistical significance was determined using a one-way analysis of variance (ANOVA) followed by the Tukey–Kramer post-hoc test (****$p < 0.0001$).

References for Supplemental Information

1. Sato Y, Mii A, Hamazaki Y, Fujita H, Nakata H, Masuda K, et al.: Heterogeneous fibroblasts underlie age-dependent tertiary lymphoid tissues in the kidney. JCI Insight 1: e87680, 2016 doi: 10.1172/jci.insight.87680
2. Sato Y, Oguchi A, Fukushima Y, Masuda K, Toriu N, Taniguchi K, et al.: CD153/CD30 signaling promotes age-dependent tertiary lymphoid tissue expansion and kidney injury. J Clin Invest 132: e14607, 2022 doi:10.1172/JCI146071
3. Concordet JP, Haeussler M: CRISPOR: Intuitive guide selection for CRISPR/Cas9 genome editing experiments and screens. Nucleic Acids Res 46: W242-W245, 2018 doi:10.1093/nar/gky354
4. Kirita Y, Wu H, Uchimura K, Wilson PC, Humphreys BD: Cell profiling of mouse acute kidney injury reveals conserved cellular responses to injury. Proc Natl Acad Sci U S A 117: 15874–15883, 2020 doi: 10.1073/pnas.2005477117